New design methodology for the calculation of the feed sections into which the acceleration track of a hyperloop vehicle is divided

Gustavo Navarro*, Marcos Blanco, Jorge Nájera, Marcos Lafoz, Eduardo Rausell, Valentín Urda

Centro de Investigaciones Energéticas, Medioambientales y Tecnologías (CIEMAT), Madrid, Spain * gustavo.navarro@ciemat.es

Acknowledgements

The authors would like to acknowledge the support from the company ZELEROS by providing the specification and characteristics related to its product. It was essential for the development of this work.

Keywords

«Sustainable technology», «Railway Power Supply», «E-Mobility», «Power Supply», «Switched reluctance drive».

Abstract

This paper presents the design methodology used to optimize the number of sections into which the acceleration track of a Hyperloop-type vehicle is divided. In these types of vehicles, a preacceleration system is necessary to reach a speed close to cruising speed before the main propulsion system can operate. For this purpose, a switched reluctance linear motor (LSRM), divided into what are called unitary machines (UMs) connected in series, is proposed along with a converter to control thrust force generated by the motor. The methodology is applied to a specific case (mission) where a mass of 250 kg needs to be accelerated over a distance of 60 m to reach a speed of 120 km/h. As a result of the proposed methodology, the number of sections into which the linear motor is divided, the number of UMs per section, and the optimal turn-on and turn-off angles of the LSRM phases are determined to achieve the target force profile.

I. Introduction

The rapid pace of technological advancement in the 21st century has significantly transformed various aspects of human life, with transportation being one of the most dynamic and evolving sectors. As cities expand global connectivity becomes increasingly vital, there is a pressing need for innovative transportation solutions that are not only faster but also more sustainable and efficient. Unfortunately, as reported by the European Environmental Agency, in 2016 the transport sector accounted for 27% of the total greenhouse gas emissions in Europe [1]. Various European policies have set goals to reduce these emissions by two-thirds by 2050, compared to 1990 levels, in order to achieve the long-term target of a 60% reduction in greenhouse gas emissions outlined in the 2011 Transport White Paper. In response to these challenges, the concept of Hyperloop was introduced in 2013 [2] as a new ultra-fast, magnetically levitated train traveling through a low-pressure tube to drastically reduce travel times between major cities while minimizing environmental impact. This system involves passenger pods or capsules traveling through a network of low-pressure tubes at speeds exceeding 700 miles per hour (1,120 kilometers per hour). By eliminating air resistance and reducing friction through magnetic levitation, the Hyperloop aims to achieve unprecedented levels of speed and efficiency.

The Hyperloop also holds the promise of reducing traffic congestion, which is a major issue in urban areas worldwide. High-speed rail systems have been proposed as a solution, but they come with significant costs and limitations in terms of infrastructure and speed. The Hyperloop, with its minimal land footprint and ability to integrate with existing urban environments, offers a more viable alternative.

However, the path to making the Hyperloop a reality is not without its challenges. Significant technical, financial, and regulatory hurdles must be overcome before the system can be widely implemented. For instance, the construction of the necessary infrastructure involves substantial

capital investment, and there are concerns about the safety and reliability of such a high-speed system. Additionally, the regulatory framework for a new mode of transportation, especially one as novel as the Hyperloop, is still under development. Governments and private companies must collaborate closely to address these challenges and ensure that the system meets the highest standards of safety, efficiency, and accessibility.

In conclusion, the Hyperloop represents a bold leap forward in the quest for faster, more efficient, and sustainable transportation. Its potential to revolutionize long-distance travel, reduce environmental impact, and alleviate urban congestion makes it one of the most exciting developments in modern transportation. While significant challenges remain, the ongoing advancements in technology and infrastructure suggest that the dream of Hyperloop travel may soon become a reality, ushering in a new age of transportation. Currently, there are multiple technological developments based on this concept [3], with projects in America [4], Europe [5], and Asia [6]. The Hyperloop idea bears some resemblance to the very-high-speed trains developed in the 20th century, such as MAGLEV trains [7][8]. The technology involves a railway line enclosed within a pressurized tube, where capsules or pods travel at intervals of 2 to 6 minutes. The operational scope for this technology, both for freight and passenger rail services, is designed to cover distances of up to 1000 km at speeds between 700 and 1000 km/h [9][10].

One of the key challenges in powering this transportation system is that, due to its extremely high speed, the moving components (pods) cannot rely on traditional pantograph systems for power supply. In this case, the most widely adopted solution is a linear motor placed along the track. In this setup, the active part, consisting of electric coils, is embedded in the track, while the passive component of the motor is mounted on the pod itself. Moreover, such high speeds would generate too much friction between the moving pods and the rail, making the use of wheels impractical. As a result, some form of levitation is essential for the system to function effectively.

The paper is structured as follows: Section II describes the approach for Hyperloop on which the design methodology is based; Section III details the proposed design methodology for calculating the power supply sections into which

the linear motor will be divided; Section IV presents the simulation results and the selected solution for the definition of the sections; and Section V outlines the conclusions drawn from the study.

II. Description of the approach for Hyperloop concept

After introducing the general principles of Hyperloop, different developers propose varying technical details. Examples of this technology already in use include the Transrapid and the Japanese JR-Maglev MLX, both of which employ magnetic levitation (MAGLEV) systems. All MAGLEV trains, as well as some Hyperloop technological concepts, rely on a linear motor for propulsion, which requires a continuous power supply along the entire track. This involves a complex network of high-voltage power lines and electronic converters, power significantly increasing infrastructure costs.

In contrast, the approach proposed by the spanish company Zeleros is different from those mentioned above. Zeleros company proposed solution consists of a rail system divided into three main sections, as illustrated in Figure 1:



Fig. 1: Track scheme with the different areas for acceleration, constant speed and deceleration

- a) Acceleration Phase: The first section, spanning between 5 and 10 kilometers, is where the pod is accelerated using a linear motor positioned along the rail. During this phase, the capsule reaches nearly its maximum speed. While there are various options for the traction motor, the preference is for a design with minimal weight in the moving components and simpler coil structures along the track.
- b) Cruise Speed Phase: In the second section, the capsule maintains its top speed. To offset any energy losses an on-board propulsion system powered by a reaction turbine is employed. In this case, a compressor at the front of the capsule draws in air, compresses it, and then expels it through the turbine. This air is used both for propulsion and levitation, reducing mechanical friction. Energy for this process is supplied by batteries installed within the capsule.
- c) **Deceleration Phase:** Finally, when the pod arrives at the destination, it needs to be

braked in a third area using regenerative braking to recuperate part of the kinetic energy of the capsule. Additional braking systems are installed at the capsules to act in case of emergency. Figure 2 illustrates the technology developed by the spanish company ZELEROS (based in Valencia, Spain), which is used in this paper as a case study to examine the power supply for this application.



Fig. 2: Technology for a Hyperloop train from the company ZELEROS

III. Design methodology of the entire acceleration system

This section describes the methodology followed for the design of the acceleration system for the manufacturing of a prototype acceleration track on a reduced scale. Before launching a commercial line, the initial phase proposed by the company Zeleros involves testing a scaled-down prototype to confirm the feasibility of the technology. For this purpose, a mission has been defined. The objective is to accelerate a mass of 250kg for 60 metres and reach a speed of 120km/h (Mission 1). There will be an additional track of 30m for braking. The complete system design methodology comprises the following steps: 1) Selection and design of the linear motor, 2) Calculation of the number of sections of the acceleration track and 3) Design of a model for the optimization of the on and off angles (α_{ON} and α_{OFF}) of the electric machine phases in order to maximize real force developed by the machine to achieve the objective (250kg, 60m, 120km/h). Figure 3 shows an outline of the characteristics of this mission:

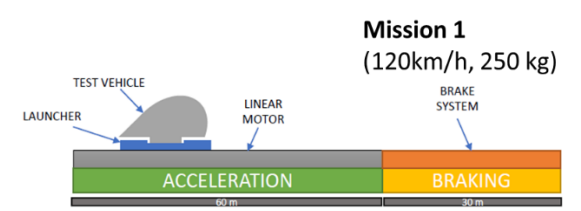


Fig. 3: Summary scheme of mission 1 considered with the value of some important parameters.

Selection and design of the Linear Motor

In this case, the need to minimize the weight of the moving components has led to the decision to place the coils of the linear motor, referred to as the active part, directly on the track. Linear motion systems (LMSs) typically use either synchronous asvnchronous or motors. Synchronous motors are more common, as seen in the Shanghai airport shuttle in China and JR systems in Japan, but they are costly for long tracks. While asynchronous motors are more affordable, they generate excessive on-board losses. As a viable alternative, the use of a switched reluctance machine is proposed. Although it offers lower overall performance, it provides significant advantages by reducing both costs and material usage, while still enabling the transport of large capacities at high speeds. Key benefits of this linear motor technology include a lightweight on-board component with low energy losses, durability, high force density, and the ability to continue operating in degraded mode if any of the phases fail. Figure 4 illustrates the proposed 6/4-pole linear switched reluctance motor, featuring translator poles (moving part) and stator poles with coils (passive part). The acceleration track requires a linear motor for a 60m reduced-scale prototype.

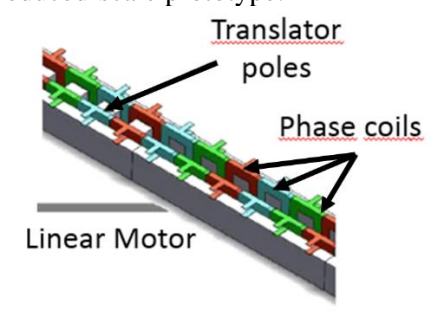


Fig. 4: Layout of 6 /4 poles LSRM with the phase coils (fixed part) and translator poles (mobile part).

Based on the specifications outlined above (Mission 1) and dynamic calculations, a preliminary design of the linear motor is created. The motor must be capable of delivering the required thrust force. This preliminary design is followed by a more detailed analysis of the electromechanical variables using finite element methods (FEM) in an iterative process to verify whether the motor can provide the required thrust force ($F_{thrust} = f(I)$). Figure 5 shows the electromagnetic analysis of the proposed 6/4-pole switched reluctance linear motor, which corresponds to the specific prototype discussed in the following section.

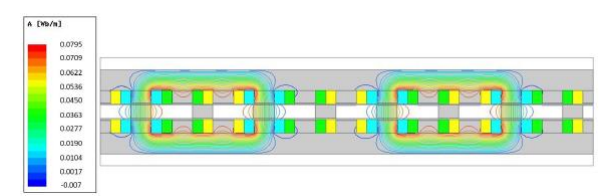


Fig. 5: Electromagnetic analysis of the designed LSRM with the magnetic flux lines path and value in Wb/m.

To power this motor, a three-phase full-bridge topology-based power electronic converter was selected. This power converter makes it possible to regulate the current through the phases of the electrical machine. In this case, a band hysteresis current control is used. Figure 6 provides an example of the operation and current waveforms for a linear switched reluctance machine (LSRM) [11][12][13][14].

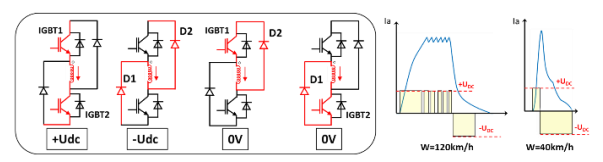


Fig. 6: Switched reluctance machine (SRM) power converter topology and current waveforms for low speed and nominal speed.

Calculation of the number of sections of the acceleration track

Based on the system dynamics and fundamental data, the theoretical number of sections into which the acceleration track is divided will be calculated. Figure 7 shows a schematic of the layout with the accelerator track divided into sections and the power converter feeding the linear motor phases. The switchers allow to have only one section powered during the acceleration.

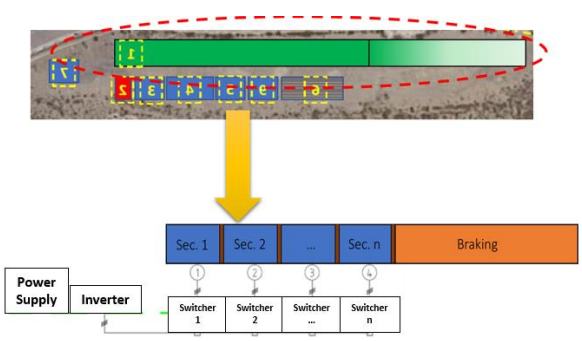


Fig. 7: Plan and schematic of the layout of the sections and power supply system.

Each section will be composed of a number of unitary machines. As discussed above, the proposed linear motor is a 6/4-pole switched reluctance machine (3 pairs of poles in the active

part and 4 poles in the moving or translator part). This configuration (6/4) is what is considered a unitary machine (UM). Figure 8 (a) shows the scheme with some dimensions of a SRM unitary machine.

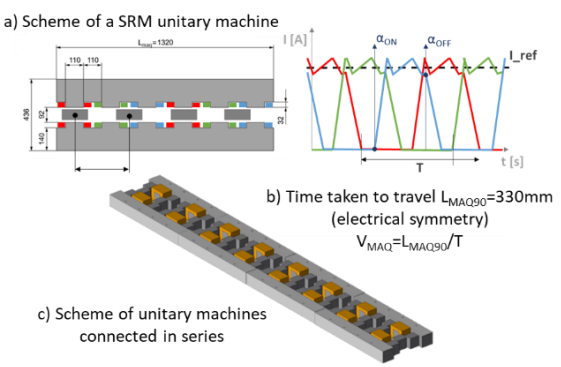


Fig. 8: a) Schematic diagram of a unitary machine; b) Time profiles of the currents; c) 3D schematic diagram of the SRM connected in series.

The total length of a UM is 1320 mm, so the total number of unitary machines on the acceleration track (60 m) will be 46. The number of sections and the number of unitary machines per section will be determined by the available voltage applied to each phase of the electrical machine to drive the current. If the voltage is insufficient, no unitary machine can be connected to that section, and a new section must be started. Since the motor's thrust force depends on the current flowing through the electrical phases, it is essential to determine the minimum voltage on the DC bus that allows the current to reach the desired value at any given moment [13][14]. Equation 1 illustrates the variables that influence the evolution of phase currents in a switched reluctance motor.

$$\frac{\partial i}{\partial t} = \frac{U_{DC} - U_R - U_L - U_V}{L(x, i)} \tag{1}$$

where:

 $\frac{\partial i}{\partial t}$: Evolution of the current over time

 U_{DC} : DC bus voltage

 U_R : Voltage drop due to resistance of wires and winding

 U_L : Voltage drop due to winding inductance

 U_V : Voltage drop due to the electromotive force of the machine.

L(x, i): Instantaneous inductance dependent on the current and the position of the tranlator poles relative to the stator poles

It must be taken into account that, at any given moment, the active section will contain unitary machines in which the stator poles and the moving part poles are aligned (active unitary machines). However, there will also be others that, despite being powered, have their magnetic flux closed through the air (passive unitary machines). Figure 9 presents a schematic where the pod is in section n, and some poles of the active part of the electrical machine are powered but not aligned with the transistor poles. These passive machines will cause an additional voltage drop, limiting the number of unitary machines that can be connected in series per section.

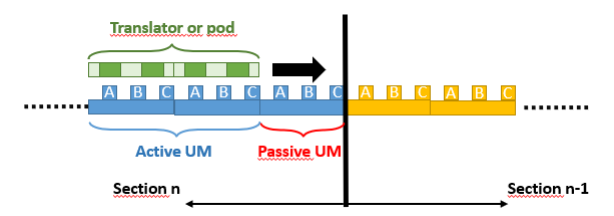


Fig. 9: Schematic of the capsule or moving part circulating through a powered n-section

Design of a model for the optimization of the on and off angles of the electrical machine phases (α_{ON} and α_{OFF})

After defining the electric motor and the theoretical number of power sections, a MATLAB-Simulink model is developed. This model includes the DC voltage bus, the power electronics converter, a complete linear motor model, and the theoretical number of sections into which the acceleration track is divided. Using this model, it will be possible to optimize the on and off angles of the electric machine phases to maximize the thrust force generated by the motor (see Figure 8c). Additionally, the model will allow for the determination of the number of sections, the number of unitary machines per acceleration section, and, consequently, the actual force produced by the machine to achieve the target parameters (250 kg, 60 m, 120 km/h)..

Figure 10 shows the MATLAB-Simulink model developed for sections calculation. The following elements are distinguished: 1) Control system: hysteresis band current control, 2) Power electronics and levitation system, 3) Complete model of LSRM.

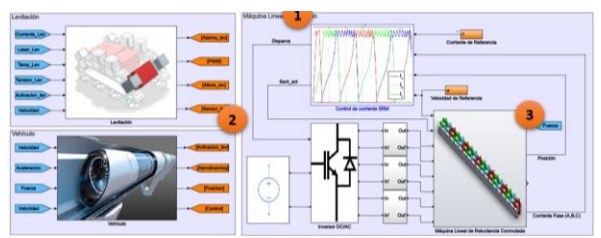


Fig. 10: Schematic of MATLAB-Simulink model developed for the design of the sections.

The model parameters that can be modified to achieve mission 1 objectives are shown in the table below:

Table I: Parameterisable variables in the model

Table 1: I drameterisable variables in the model	
Electrical machine and section parameters	
Number of turns per coil	$N_{\rm f}$
Number of passive unitary machines per section	N _{pas}
Current through the phases of the linear	I_{ref}
motor	
Wiring resistance	R
Number of active unit machines per section	Nact
Correction factor for section change	K _{sec}
Magnetic flux and mechanical force tables	Θ, F
Skin effect on cables as a function of speed	δ
Mission parameters	
Minimum target force profile to meet the	F_{ref}
speed	
Mass of the pod	M
Target speed	v
Parameters related to the power system	
DC power supply voltage	V_{DC}
Maximum current through linear motor	I _{max}
phases	
Hysteresis bandwidth	ΔI
Characteristics of power modules for	η
efficiency	
Phase on/off angles as a function of speed	$\alpha_{on/off}$

Regarding the parameters listed in Table 1, some are set to the following values:

- 1. Maximum DC supply voltage (VDC): 1000V
- 2. Maximum reference current (Iref): 450A
- 3. **Nf** = 22 turns per coil (unitary machine force and flux table)
- 4. Total resistance (coil + connection cable): $136.8 \text{ m}\Omega$
- 5. **Force profile (F)** as a function of velocity and position

Once certain parameter values are defined, a parametric analysis is conducted. To achieve this, a series of vectors is created for specific variables, each with a predefined set of parameter values. Each combination of these vector values represents a simulation case. In this study, the variables parameterized in the simulation are:

- 1. Mass velocity along the acceleration track (v)
- 2. Number of unitary machines connected in series per section (N° UM)

- 3. Linear motor phase on-angle (α_{ON})
- 4. Linear motor phase off-angle (α_{OFF})

The primary output variable evaluated in each simulation case is the average force, while additional variables such as maximum and minimum current are also recorded. The vectors containing the modified parameter values are as follows:

- v (m/s) = [6.3, 11.9,..,34.95]-> **16** param.
- $N^{\circ}UM = [2, 4, 6, \dots, 44, 48] -> 15 \text{ param}.$
- $\alpha_{OFF}(^{\circ}) = [20:1:45] > 26 \text{ param}.$
- $\alpha_{ON}(^{\circ})=[-40:1:0]->$ **41 param**.

A total of 16x15x26x41 = 255,840 operating conditions were analyzed by simulating the linear motor with a constant reference current (450 A). Once the 255,840 simulations were completed in MATLAB-Simulink, the results were grouped by speed (v) and the number of unitary machines (N° UM). The average force developed by the linear motor for each pair of speed values and number of unitary machines was then plotted as a function of the on/off angles (α_{ON}/α_{OFF}) of the phases. The total number of graphs is 16x15 parameters = 240cases. For each simulation case or force value, the maximum current error (I_{max}/I_{ref}) and the minimum current error (I_{min}/I_{ref}) were calculated. These errors are defined to assess the dynamic performance of the linear motor. Figure 11 (left) shows the case when the current through the machine's phases does not reach the reference value, and (right) shows the case when the current in the switched-off phase does not reach zero. In the first case, there is a maximum current error because the current through the phases does not reach the reference value.

In the second case, there is a minimum current error because the current through the non-active phases is not extinguished before they are switched on again. The first error (I_{max}/I_{ref}) should be close to unity, and the second error (I_{min}/I_{ref}) should be close to zero. The first case implies that the inductances of passive machines—those in the fed section where the magnetic flux does not circulate through the translator or moving part—and the counter-electromotive force prevent the current from reaching the reference value.

On the other hand, the second case implies higher losses due to the Joule effect and added difficulty in transitioning between the section to be fed and the new section to be fed, as the current must be zero to perform this transition. The results obtained from the simulations are presented in the following section.

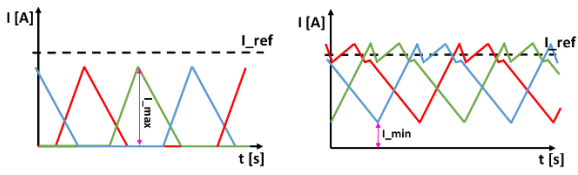


Fig.11: Schematic of current evolutions in the SRM and calculation of maximum (left) and minimum current errors (right)

IV. Simulation results

From the 240 cases mentioned above, it is possible to determine the angle values (α_{ON} and α_{OFF}) that optimize the force value (F_{MAX}) for each pair of speed (v) values and number of unit machines (N° of UMs). For example, Figure 12 shows the force map as a function of α_{ON} and α_{OFF} for a speed of 15.9 m/s and 8 unit machines connected in series. On the other hand, Figure 13 displays the same force map as a function of α_{ON} and α_{OFF} for a speed of 15.9 m/s, but with 24 unit machines connected in series. In these graphs, the black contour lines represent the minimum current error (I_{min}/I_{ref}).

Additionally, the graphs show the value of the maximum force without any restriction as a blue circle, and the value of the maximum force when a restriction is imposed on the minimum current error $(I_{min}/I_{ref}) < 0.05$. In this case, the minimum current (Imin) will be at most $0.05 \cdot 450 = 22.5$ A. In Figure 12, the maximum force value without restrictions (blue circle) and the maximum force value with the restriction $(I_{min}/I_{ref} < 0.05)$ coincide and occur at the same turn-on and turn-off angles. However, in Figure 13, the two force values—without and with constraints—occur at different turn-on and turn-off angles.

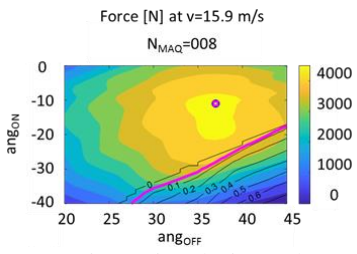


Fig. 12: Grouping simulations by number of unitary machines in series (8) and speed 15.9m/s

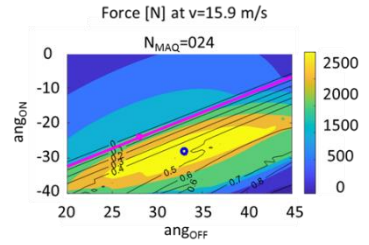


Fig. 13: Grouping simulations by number of unitary machines in series (24) and speed 15.9m/s

In this way, for each speed value, 15 graphs are obtained (one for each elements of the UM vector) showing the force level curves as a function of the on and off angles (α_{ON} and α_{OFF}). Figure 14 shows the 15 curves obtained for a speed of 6.4m/s as a representative example.

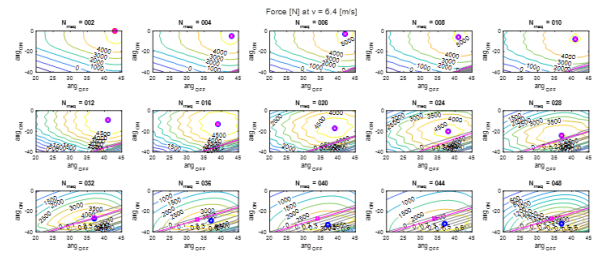


Fig. 14: Force results grouped by a constant speed of 6.4m/s and 15 cases of number of UM connected in series

From these graphs, a family of curves can be obtained, where the force value as a function of speed is plotted for different numbers of unit machines connected in series [2, 4, 6, ..., 44, 48]. In total, 30 force profiles (F_{MAX} and F_{MAX} with constraints) are plotted as a function of speed. Figure 15 shows the force profile with and without constraints as a function of speed for different numbers of unit machines connected in series. The graph displays the force values, both with and without constraints, for the case of 24 unit machines connected in series and a mass velocity of 15.9 m/s, represented by blue and magenta circles.

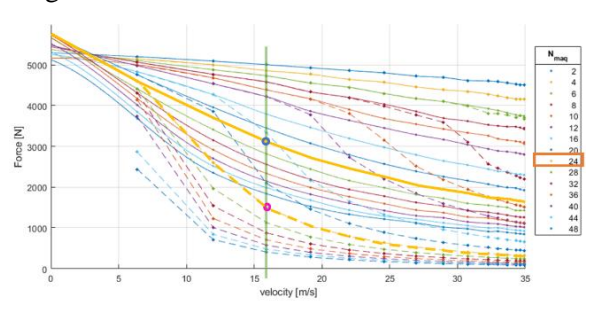


Fig. 15: Evolution of force as a function of speed for different number of machines in series (both optimal and with minimum current restrictions)

As previously mentioned, the process begins with a target force profile based on position and speed. Additionally, the acceleration section length (60 m) and the number of unit machines (46) that fit within this section, given the length of each unit machine (1.320 m), are known. The goal is to determine the number of sections and the number of unit machines connected in series per section that allow the linear motor to provide at least the target force while adhering to the previously mentioned restriction, Imin/Iref < 0.05. Figure 16

shows a schematic of the sections of the acceleration track. A brute-force approach is used to optimize the section calculation. The bruteforce optimization process for this purpose is illustrated in the diagram on the left side of Figure 17. The process starts at the end of the track with section 1, where the maximum number of unit machines connected in series is determined, ensuring that the motor delivers a force above the target value. At the top right of Figure 17, a graph shows the target force profile based on position in red, along with the number of unit machines connected in series that enable the system to reach at least the target force. This is achieved with 2, 4, 6, 8, or 10 unit machines. Among these values, the highest is selected, since a greater number of unit machines connected in series that meet the target force requirement will reduce the number sections needed, thereby minimizing transitions between sections, decreasing force loss, and lowering costs.

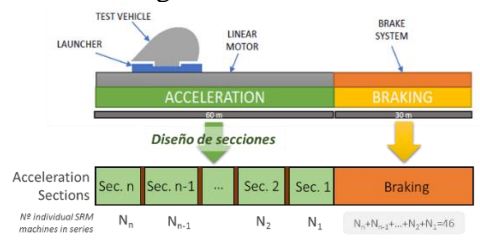


Fig. 16: Schematic with the sections of the acceleration track

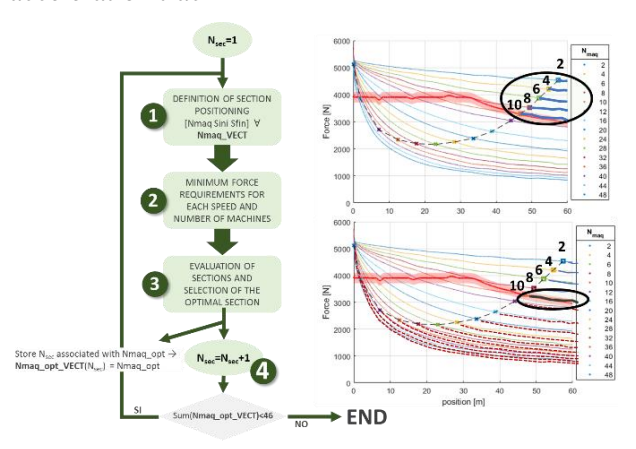


Fig. 17: Outline of the section design procedure and force curves as a function of position and velocity for the design of section 1.

Once the number of unit machines for section 1 is selected, the algorithm begins the same process for section 2, starting from where section 1 ended. This position is calculated as: $60(m) - 10(U.M.) \cdot 1.320(m / U.M.) = 46.8m$. The process is repeated iteratively until the entire available acceleration length is completed. Figure 18 shows the power profile as a function of

capsule position for the selected solution, with the number of unit machines connected in series [10, 10, 8, 8, 10] in each of the 5 sections into which the acceleration segment is divided. Throughout the process, the theoretical force profile of the linear motor (black lines) with this configuration remains above the target profile (in red), except at the end of section 2, where the force is slightly below the target value. This is compensated for by section 1, where the linear motor force is significantly above the target value. Figure 19 shows the same power profile for the selected solution, but in this case, it is plotted as a function of pod velocity.

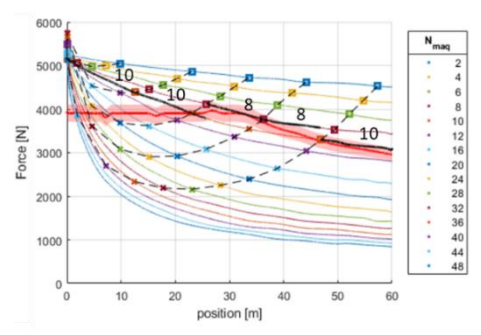


Fig. 18: Power profile as a function of the position resulting from the section design carried out.

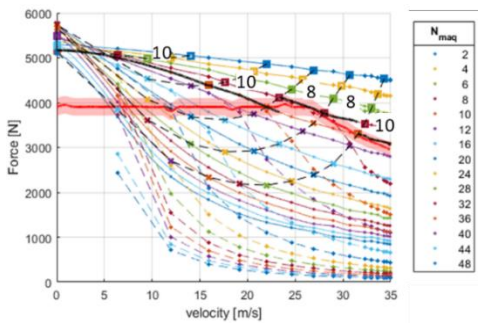


Fig. 19: Power profile as a function of speed resulting from the section design carried out

Finally, Figure 20 shows a real image of a part of the LSRM acceleration track that Zeleros is testing in its facilities.



Fig. 20: A real image of the acceleration segment with LSRM that the company Zeleros has at its facilities.

V. Conclusion

This article presents the procedure used to calculate the sections of the acceleration segment for a Hyperloop-type vehicle, employing a switched reluctance linear motor. The process begins with defining the speed and distance objectives for a given mass. From there, the force profile along the acceleration segment is selected. Several parameters are also set, such as the number of turns per coil in the active part of the linear motor, which in this case is 22. Before proceeding with the design, the existing criteria for determining the number of sections are analyzed: 1) minimizing the number of sections, or 2) ensuring the target force is provided.

The section design solution is chosen based on the criterion of providing at least the target force for each speed defined by the company ZELEROS. This option is selected because minimizing the number of sections would result in the theoretical force calculated closely aligning with the target profile, leaving no margin for potential issues (e.g., friction forces, reduced force in the constructed prototype, inability to reach maximum force due to control limitations, etc.). However, the downside of the selected criterion is that it leads to a higher number of sections, resulting in more transitions between sections. These transitions, in turn, create additional force gaps. The final design divides the acceleration segment into 5 sections, each containing 8 and 10 unit machines (UM) connected in series. The theoretical force profile obtained with this configuration provides a margin relative to the target profile, especially at the beginning of the track. Additionally, the force curves shown are evaluated at the nominal current (450 A) throughout the entire track, meaning that increasing the current to gain additional force is not an option.

VI. References

- [1]. European Environment Agency. Greenhouse Gas Emissions from Transport. Available online: https://www.eea.europa.eu/data-and-maps/indicators/transport-emissions-of-greenhouse-gases/
- [2]. Musk, E. Hyperloop Alpha. 2013. Available online:
 http://www.spacex.com/sites/spacex/files/hyperloopalpha-20130812.pdf
- [3]. Kale, S.R.; Laghane, Y.N.; Kharade, A.K.; Kadus, S.B. Hyperloop: Advance Mode of Transportation System and Optimize

- Solution on Traffic Congestion. Int. J. Res. Appl. Sci. Eng. Technol. (IJRASET) 2019, 7. ISSN 2321-9653
- [4]. Hyperloop One. Available online: https://hyperloop-one.com/global-challenge
- [5]. Hardt. European Hyperloop Program. 2018: https://ec.europa.eu/eipp/desktop/en/projects/project-print-9401.html
- [6]. Hyperloop Transportation Technologies.

 Available online:

 https://www.hyperloop.global/about
- [7]. Ono, M.; Koga, S.; Ohtsuki, H. Japan's Superconducting MAGLEV TRAIN. IEEE Instrum. Meas. Mag. 2002, 5, 9–15
- [8] Ikeda, H.; Kaga, S.; Osada, Y.; Ito, K.; Mugiya, Y.; Tutumi, K. Development of power supply system for Yamanashi Maglev Test Line. In Proceedings of the Power Conversion Conference—PCC'97, Nagaoka, Japan, 3–6 August 1997; Volume 1, pp. 37
- [9]. European Union Agency for Railways: Hyperloop—An Innovation for Global Transportation?

 https://www.era.europa.eu/sites/default/files/library/docs/hyperloop_innovation_for_global_transportation_en_1.pdf
- [10]. Werner, M.; Eissing, K.; Langton, S. Shared Value Potential of Transporting Cargo via. Hyperloop. Front. Built Environ. 2016, 2, 17
- [11]. Abdel-Aziz, A., Elgenedy, M., & Williams, B. (2024). Review of Switched Reluctance Motor Converters and Torque Ripple Minimisation Techniques for Electric Vehicle Applications. Energies, 17(13), 3263
- [12]. M. Deepak, G. Janaki, C. Bharatiraja, Power electronic converter topologies for switched reluctance motor towards torque ripple analysis, Materials Today: Proceedings, Volume 52, Part 3, 2022, Pages 1657-1665, ISSN 2214-7853.
- [13]. Byeong-Seok Lee, Han-Kyung Bae, P. Vijayraghavan and R. Krishnan, "Design of a linear switched reluctance machine," Conference Record of the 1999 IEEE Industry Applications Conference. Thirty-Forth IAS Annual Meeting (Cat. No.99CH36370), Phoenix, AZ, USA, 1999, pp. 2267-2274 vol.4
- [14]. N. Prasad, S. Jain and S. Gupta, "Review of Linear Switched Reluctance Motor Designs for Linear Propulsion Applications," in CES Transactions on Electrical Machines and Systems, vol. 6, no. 2, pp. 179-187, June 2022